Transition Metal Chemistry (2021) 46:91–101
https://doi.org/10.1007/s11243-020-00425-5

Synthesis, spectroscopic characterization, crystal structure and theoretical investigation of two azo-palladium (II) complexes derived from substituted (1-phenylazo)-2-naphtol

Souheila Chetioui[1,3] · Bachir Zouchoune[1,2] · Hocine Merazig[1] · Salah-Eddine Bouaoud[1,2] · DjamilAzeddine Rouag[1] · Jean-Pierre Djukic[4]

Received: 13 May 2020 / Accepted: 13 September 2020 / Published online: 20 September 2020

Abstract

The *ortho*-substituted (E)-1-((2-methoxyphenyl)diazenyl)naphthalen-2-ol and the *meta*-substituted (E)-1-((3-methoxyphenyl) diazenyl)naphthalen-2-ol were, respectively, used in the synthesis of two new complexes, bis[1-(2-methoxyphenylazo)-2-naphthoxy]palladium(II) and bis[1-(3-methoxyphenylazo)-2-naphthoxy]palladium(II), noted (I) and (II), respectively. (I) and (II) were characterized by physicochemical and spectroscopic methods, and their molecular structures were determined by X-ray crystallography. Both complexes display a square-planar geometry, which is reproduced by full geometry optimizations at the DFT/B3LYP level. Calculations were also performed on the free ligands (in their precursor form), as well as their *para*-substituted isomer (E)-1-((4-methoxyphenyl)diazenyl)naphthalen-2-ol and its hypothetical complex bis[1-(4-methoxyphenylazo)-2-naphthoxy]palladium(II) (compound (III). Calculations were also performed on the free p-phenylazo-2-naphthol ligand (p-MoxyPhNap), in order to understand their bonding and to analyze their electronic structure. TD-DFT calculations were also performed on the three complexes to simulate their absorption spectra from and compare to the experimental UV–Vis data of (I) and (II). The main peaks in the spectrum of (I) are assigned to mixed LMCT/LLCT and π–π * (ILCT) transition, while the unique major peak afforded by (II) is assigned to MLCT and LLCT transitions.

Introduction

Transition metal complexes of azo compounds have received increasing interest in both basic and applied research, owing to their peculiar electronic and structural characteristics and their relationships with their use in different crucial fields [1–4], privileged by their low cost. The transition metal-azo dye complexes are related to the possibility to obtain new compounds with various biological activities [5, 6]. This class of complexes is important in the progress of metal-based anticancer agents [7, 8]. These different areas of interest fostered inorganic chemists to develop novel approaches to the preparation of non-covalently bound anticancer drugs [9, 10].

There is a great coordination affinity of the metals toward chromophoric ligands, leading to the formation of transition metal complexes evidenced by an absorption displacement of their UV–Vis spectra and accompanied by an enhancement of the dye fastness [11–13]. Various properties such as structures, chelate formation constants, and stability have been reported [14]. Different classes of chromophoric ligands, particularly those characterized by the presence

This paper is dedicated to Dr. Jean-René Hamon at the occasion of his 65th birthday.

Electronic supplementary material The online version of this article (https://doi.org/10.1007/s11243-020-00425-5) contains supplementary material, which is available to authorized users.

✉ Bachir Zouchoune
bzouchoune@gmail.com

[1] Unité de Recherche de Chimie de L'Environnement Et Moléculaire Structurale, Université Constantine Mentouri, 25000 Constantine, Algeria

[2] Laboratoire de Chimie appliquée Et Technologie Des Matériaux, Université Larbi Ben M'Hidi - Oum El Bouaghi, 04000 Oum El Bouaghi, Algeria

[3] Université Mohamed Boudiaf-M'Sila, M'Sila, Algérie

[4] Laboratoire de Chimie Et Systémique Organométallique(LCSOM), Institut de Chimie, Université de Strasbourg, UMR 7177, 67070 Strasbourg Cedex, France

of the azo group (–N = N–), have been applied as chelate indicators to identify metal ions, where the complex formation is related to a change of color [15–18]. Due to their easy use, several areas of application have emerged into numerous high-technological frontier applications such as high-density memory storages (CD-R and DVD-R) [19–21], which is considered as an important and promising branch of chemistry with significant physicochemical and material properties.

Recently, Pd-arylazo complexes have found application in C–C coupling reactions [22, 23] interacting strongly with CT DNA [24] and exhibiting photochromic activity [25, 26], where most of their electronic and photochromic efficiency have been explained by DFT calculations.

We report two novel Pd(II) coordination complexes obtained using (E)-1-((2-methoxyphenyl)diazenyl)naphthalen-2-ol [27] and (E)-1 ((3methoxyphenyl)diazenyl) naphthalen-2-ol [28] azo-ligands. These two bidentate ligand precursors are isomers differing from the *ortho versus meta* position of their methoxyphenyl group. In both Pd(II) complexes (I) and (II), respectively, the metal is coordinated to two N atoms and two O atoms. The experimental studies were performed on the *meta* ligand precursor in both ketonic and enolic forms under variable temperatures. To our knowledge, there are no other complexes with similar ligands bearing methoxy groups reported in the literature. In all the investigated complexes, the metal coordination mode is almost perfectly square-planar.

Experimental section

Materials and methods

Elemental analyses (C, H, N) were performed on a Vario EL III elemental analyzer. UV spectra were recorded on an Agilent UV–VIS spectrophotometer 8453 (spectroscopy system) with G1120A multicell transport and a computer with ChemStation (G Visible Ultra Violet 1120 A). Infrared spectra were recorded with a Fourier transform infrared spectrometer (ALPHA) FTIR from the brand BRUKER controlled by Opus 6.5 software and fitted with an Attenuated Total Reflectance (ATR) accessory in diamond crystal. The ^{1}H NMR spectra were recorded in deuterated chloroform $CDCl_3$ with infinite dilution at high fields on a Brücker Avence DPX-type spectrophotometer, 400 MHz, TMS as internal reference, chemical shift in ppm. The diffraction data were collected on a Nonius Kappa CCD diffractometer using graphite monochromatized Mo-Kα radiation (λ = 0.71073 Å).

Preparation of complex (I)

Complex (I) was prepared as described in Scheme 1. A mixture of $Pd(AcO)_2$ (0.056 g, 0.25 mmol) was dissolved in hot methanol (10 ml), added to the ligands (E)-1-((2-methoxyphenyl)diazenyl)naphthalen-2-ol (0.33 g,0.5 mmol) and dissolved in hot methanol (25 ml). The color of the solution changed to dark red after the addition. The reaction mixture was refluxed overnight (24 h) and then evaporated until 30% of the total volume of the reaction solution remained at the end of the reaction. The solvent was removed under vacuum and the residue was washed twice with hexane to give dark red solids (70%). The resulting solids were crystallized from CH_2Cl_2 to yield dark red prismatic-like crystals.

Elemental analysis: N (7.76%), C (62.03%), H (3.77%) and calculated N (8.48%), C (61.78%), H (3.96%).IR (cm^{-1}):υ(N = N); 1372 cm^{-1}, υ (C–N); 1146 cm^{-1}, υ (C–O); 1213 cm^{-1},υ (C = C) aromatic; 1470 cm^{-1},υ (C–H) aromatic; 2937 cm^{-1},υ (Pd–N); 464 cm^{-1},υ (Pd–N); 579 cm^{-1} (Figure S1a). ^{1}H NMR ($CDCL_3$-d_1, δ ppm): 3.70 (s, 6H, OCH_3), 7.01–7.64 (m, 20H, Ph) (Figure S2a).

Preparation of complex (II)

Complex (I) was prepared as described in Scheme 2. A mixture of $Pd(AcO)_2$ (0.056 g, 0.25 mmol) was dissolved in hot methanol (10 ml), added to the ligands (E)-1-((3-methoxyphenyl)diazenyl)naphthalen-2-ol (0.33 g,0.5 mmol) and dissolved in hot methanol (25 ml). The color of the reaction solution changed to dark red after the addition. The reaction mixture was refluxed (24 h) overnight and then evaporated until 30% of the total volume of the reaction solution remained at the end of the reaction. The solvent

Scheme 1. Reaction route for the Pd(II) complex(I)

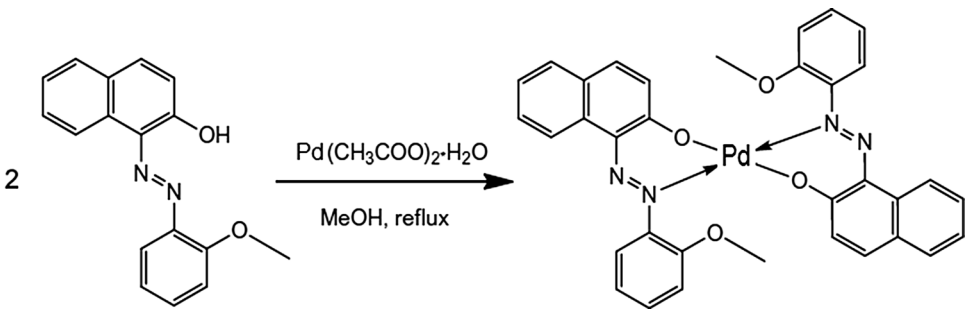

Scheme 2. Reaction route for the Pd(II) complex(II)

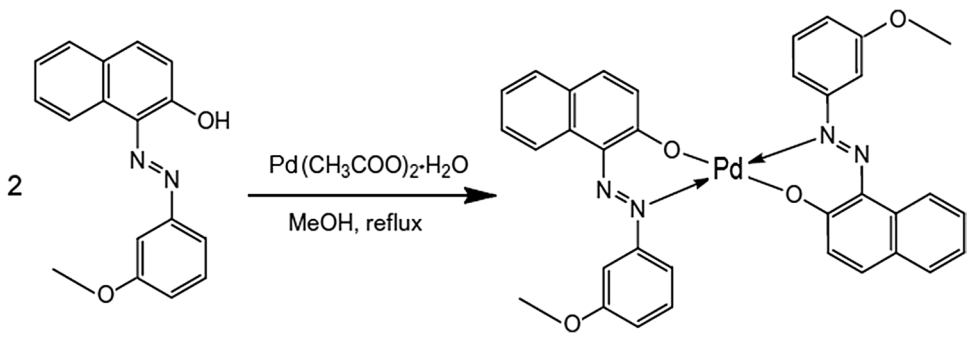

was removed under vacuum, and the residue was washed twice with hexane to give dark red solids (73%). The resulting solids were crystallized from CH_2Cl_2 to yield dark red plate crystals.

Experimental results: Found (%): N (8.45%), C (62.08%), H (3.99%) and Calculated (%)N (8.48%), C (61.78%), H (3.96%). The IR spectrum of the complex (Figure S1b of the Supporting data) shows the vibration bands: υ(N = N); 1399 cm^{-1}, υ (C–N); 1130 cm^{-1}, υ (C–O); 1213 cm^{-1},υ (C = C) aromatic; 2937 cm^{-1},υ (C–H)aromatic;2963 cm^{-1},υ (Pd–N); 446 cm^{-1},υ (Pd–O); 582 cm^{-1}.

^{1}H NMR ($CDCL_3$-d_1, δ ppm): 3.84 (s, 6H, OCH_3), 7.21–7.61 (m, 20H, Ph). (Figure S2b of the Supporting data).

X-ray crystallography

Single crystal X-ray structural analysis

A single crystal was carefully selected under a polarizing microscope in order to perform its structural analysis by X-ray diffraction. The diffraction data were collected on a Nonius Kappa CCD diffractometer using graphite monochromatized Mo-Kα radiation (λ = 0.71073 Å). The structures were solved by direct methods using SHELXS-2014 [29] and refined against F2 by full-matrix least-squares methods with anisotropic displacement parameters for all non-hydrogen atoms. All calculations were performed using SHELXS-2014 and SHELXL-2014, implemented in the WINGX system of programs [30]. The drawings were performed using the Mercury program [31]. The refinement was done by full-matrix least squares methods (SHELXL-2014 program) and converged to an acceptable final agreement factor. The pertinent experimental details of the structure determination of the new compounds are gathered in Table 1. All hydrogen atoms were placed in idealized positions and constrained to ride on their parent atoms with C–H = 0.93 Å with Uiso (H) = 1.2 Ueq (C) for aromatic hydrogen; C–H = 0.96 Å with Uiso (H) = 1.5Ueq(C) for CH_3-group. Crystal data and structure refinement parameters for complexes (I) and (II) are listed in Table 1.

Computational methods

All geometry optimizations were performed using the 2016.01 version of the Amsterdam Density Functional (ADF) program [32] developed by Baerends and co-workers [33–37] by means of the hybrid-type B3LYP functional (Becke's three parameter hybrid exchange functional [38] coupled with the Lee–Yang–Parr nonlocal correlation functional) [39]. The atom electronic configurations were described by a triple-ζ Slater-type orbital (STO) basis set for H 1 s, C 2 s and 2p, N 2 s and 2p, O 2 s and 2p augmented with a 3d single-ζ polarization for C, N and O atoms and with a 2p single-ζ polarization for H atoms. A triple-ζ STO basis set was used for Pd 4d and 5 s augmented with a single-ζ 5p polarization function for Pd. The scalar relativistic zero-order regular approximation (ZORA) was used (with the associated optimized valence basis set) for Pd [40–42]. Vibrational frequency calculations [43, 44] were performed on all the optimized geometries to confirm that these structures are true minima on the potential energy surface. Singlet–triplet excitation energies and the transition dipole lengths were computed using TD-DFT as implemented in the Response [45] code in the ADF package.

Solvent effects were considered by using the Conductor-like Screening Model for realistic solvent (COSMO-RS) model developed by Klamt and coworkers [46]. Natural populations (NAO) are obtained by NBO calculations [47, 48]. Representations of the molecular structures and molecular orbitals were done using the ADF-GUI software [32].

Crystal structure of complexes (I) and (II)

Compound (I) crystallizes in the monoclinic crystal system (space group P21/n). It is a tetra-coordinated metal complex (Fig. 1). The Pd(II) center is surrounded by two N two O atoms which are coplanar. The metal environment exhibits a quasi-regular tetragonal coordination mode. The asymmetric unit contains one half molecule, with the Pd atom occupying the inversion center. The two N atoms and two O atoms are coplanar and trans to each other with an O1—Pd—N2 bond angle of 89.69(14)° and O1—Pd—$N2^i$ angle

Table 1 Crystallographic data and refinement parameters for complexes I and II

Compound	(I)	(II)
Formula	$C_{34}H_{26}N_4O_4Pd$	$C_{34}H_{26}N_4O_4Pd$
Formula weight (g mol^{-1})	660.99	660.99
Temperature (K)	173(2)	173 (2)
Crystal habit, color	Prism, red	Plate, red
Crystal system	Monoclinic	Monoclinic
Space group	P 2_1/n	P2_1/c
a (Å)	10.6196 (6)	15.9063 (10)
b (Å)	10.3855 (7)	5.2680 (2)
c (Å)	12.8983 (6)	17.5646 (11)
α (°)	90	90
β (°)	90.947 (3)	114.683 (2)
γ (°)	90	90
Volume ($Å^3$)	1422.36 (14)	1337.34 (13)
Z	2	2
Density (calculated, g cm^{-3})	1.543	1.641
Absorption coefficient (mm^{-1})	0.7	0.744
F(000)	672	672
Crystal size (mm)	0.05 × 0.20 × 0.32	0.05 × 0.14 × 0.50
θ range for data collection (◦)	2.518– 27.470	2.819–27.415
Reflections collected	10,643	5311
Independent reflections	3252	3041
Reflections with I ≥ 2σ(I)	2167	1982
Rint	0.1044	0.0661
Number of parameters	197	196
Goodness of fit on F^2	1.009	0.898
Final *R* indices [I ≥ 2σ(I)]	0.0476	0.0422
R indices [all data]	$R_1 = 0.0860$, $wR_2 = 0.1098$	$R_1 = 0.0853$, $wR2 = 0.0947$
$\Delta\rho_{max}$, $\Delta\rho_{min}$ (e $Å^{-3}$)	0.66, – 1.64	0.621, – 1.09
CCDC deposition no	1,921,570	1,921,571

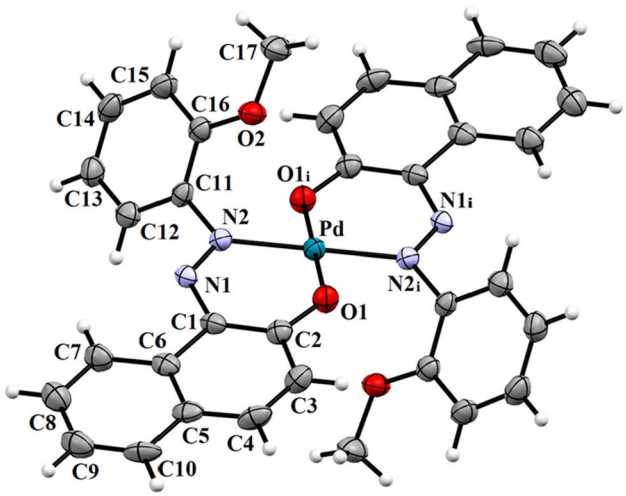

Fig. 1 The molecular structure of compound (I), with atom labeling and 50% probability displacement ellipsoids. The unlabeled atoms are related to the labeled atoms by the symmetry operation (− x + 2, − y, − z + 1)

of 90.31(14)°; symmetry code: (i) − x + 2, − y, − z + 1. The Pd—O1 and Pd—N2 bond distances are 1.976(3) Å and 1.976(3) Å, respectively (Table 2).

In the crystal, the molecules are forming chains along [100] as shown in Fig. 3. The chains are linked by C–H···π interactions, where C(17)–H(17C)…Cg1 corresponds to a distance of 2.720 Å (Table 3) giving rise to slabs lying parallel to (011). The network is characterized by the presence of weak C7–H7···N1 hydrogen bonds with relatively long H7···N1 distance of 2.450 Å, long donor–acceptor C7–N1 distance of 2.770 Å and an angle C–H–N of 100° which strongly deviates from the linearity in accordance with weak interactions.

Compound (II) crystallizes in the monoclinic crystal system (space group P21/c). As observed for compound (I), it is coordinated in a N, O-bidentate manner (Fig. 2). The metal atom is tetra-coordinated to two oxygen atoms in a trans position of the C–O function and two nitrogen atoms in a trans position to the N = N function. The geometry around the metal is almost perfectly square-planar

Table 2 Selected geometric parameters (Å, °) for complexes (I) and (II)

Bond distances (Å)			Bond angles (°)
Complex (I)			
Pd—O1	1.976 (3)	O1—Pd—N2	89.69 (14)
Pd—N2	2.004 (4)	O1—Pd—N2^{i}	180.00
Pd—O1^{i}	1.976 (3)	O1^{i}—Pd—N2	90.31 (14)
Pd—N2^{i}	2.004 (4)	N2—Pd—N2^{i}	90.31 (14)
		O1^{i}—Pd—N2^{i}	180.00
			89.69 (14)
Symmetry codes: (i) − x + 2, − y, − z + 1			
Complex (II)			
Pd—O1	2.000 (2)	O1—Pd—N2	86.41 (12)
Pd—N2	2.031 (3)	O1—Pd—O1^{i}	180.00
Pd—O1^{i}	2.000 (2)	O1^{i}—Pd—N2	93.59 (12)
Pd—N2^{i}	2.031 (3)	N2—Pd—N2^{i}	93.59 (12)
		O1i—Pd—N2^{i}	180.00
			86.41 (12)

Table 3 Interatomic distances (Å) and angles (°) for complexes (I) and (II): Cg1 is the centroid of the C5–C10 ring

D–H…A	d(D–H)	d(H···A)	d(D–A)	D–H–A
Complex (I)				
C7—H7···N1	0.9300	2.4500	2.770 (6)	100.00
C17—H17C…Cg1^{i}	0.9600	2.720	3.524 (5)	141.00
Symmetry codes: (i) 3/2-x,1/2 + y,1/2-z				
Complex (II)				
C7—H7···N1	0.9300	2.4800	2.789 (5)	100.00
C15—H15···O1^{ii}	0.9300	2.5500	3.364 (5)	146.00
C16—H16···O1^{i}	0.9300	2.5000	2.885 (4)	105.00
C17—H17*A*···O2^{iii}	0.9300	2.5400	3.374 (6)	145.00
Symmetry codes: (i) $-x+2, -y, -z+2$; (ii) $-x+2, -y+1, -z+2$; (iii) $-x+1, -y+1, -z+2$				

with distances between Pd(II) and O1, N1 of 2.000(2) and 2.031(3) Å, respectively, and an O1—Pd—N2 bond angle of 86.41(12)° and O1—Pd—N2^{i} angle of 93.59(12)°; symmetry code: (i) − x + 2, − y, − z + 2 (Fig. 3).

In the crystal, the molecules are linked via C–H···N and C–H···O intermolecular interactions, forming a layer parallel to (101) (Fig. 4). Indeed, C–H···O hydrogen bonds engaging the hydrogen and oxygen atoms of the methoxy groups are characterized by long H···O and C–O distances of 2.540 and 3.374 Å and a bending C–H–O angle of 145°, giving rise to weak interactions. Details of these interactions are given in Table 3.

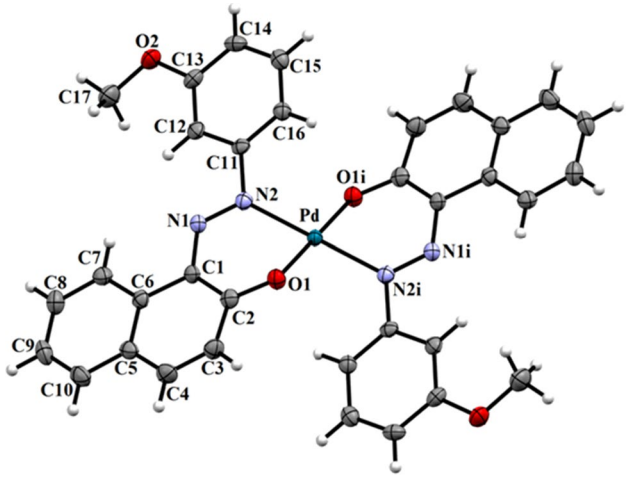

Fig. 2 The molecular structure of compound (II), with atom labeling and 50% probability displacement ellipsoids. The unlabeled atoms are related to the labeled atoms by the symmetry operation (− x + 2, − y, − z + 2)

Theoretical investigation

Geometry optimizations

The full geometry optimization of the *meta* and *para* isomers of the free ligand precursor (E)-1-((p-methoxyphenyl) diazenyl)naphthalen-2-ol ($p = 3, 4$, respectively) gave rise to almost isoenergetic structures, while the *ortho* isomer ($p = 2$) is higher in energy by 9.1 kcal/mol. The three structures are planar with comparable geometrical parameters (Fig. 5), but showing a destabilizing interaction between the oxygen atom of the methoxy group and the nitrogen atoms of the azo group that is larger in the *ortho* case, in line with its Pauli repulsion energy of 448 kcal/mol, compared to those of the *meta* and the *ortho* isomers of 418 and 422 kcal/mol, respectively.

In order to provide further understanding of the molecular structures, electronic structure and bonding, full geometry optimizations have been carried out on the Pd complexes (I), (II) and (III), deriving from the three *ortho*, *meta* and *para* precursor isomers (E)-1-((p-methoxyphenyl)diazenyl) naphthalen-2-ol ($p = 2, 3, 4$), respectively. Whereas (I) and (II) have been characterized (see above), (III) is unknown so far. The three complexes are of C_i symmetry and exhibit a square-planar geometry around the metal center (Fig. 6). The two substituted azo ligands are related through the inversion center at the Pd(II) center, which is bonded to two N and two O atoms, in a manner similar to related experimentally characterized complexes [49, 50]. In particular, there is a good agreement between the optimized and experimental (see above) structures of (I) and (II). Whereas (II) and (III) are close in energy, (I) is less stable. This instability

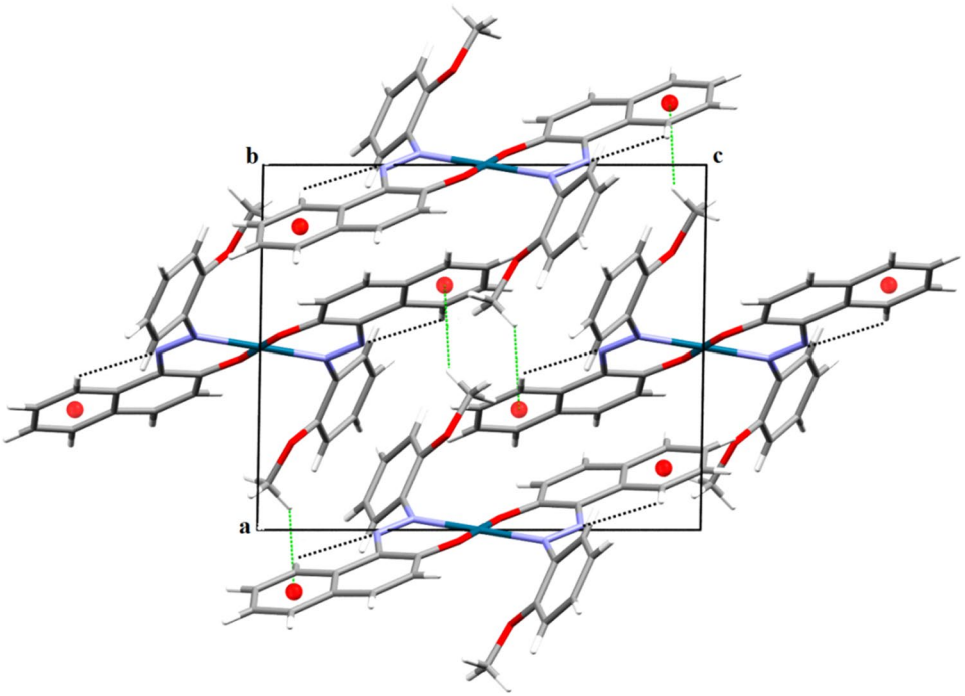

Fig. 3 A partial view along the b axis of the crystal packing of the title complex (I), displaying the C–H···N and C–H···π interactions as dashed lines (see Table 3)

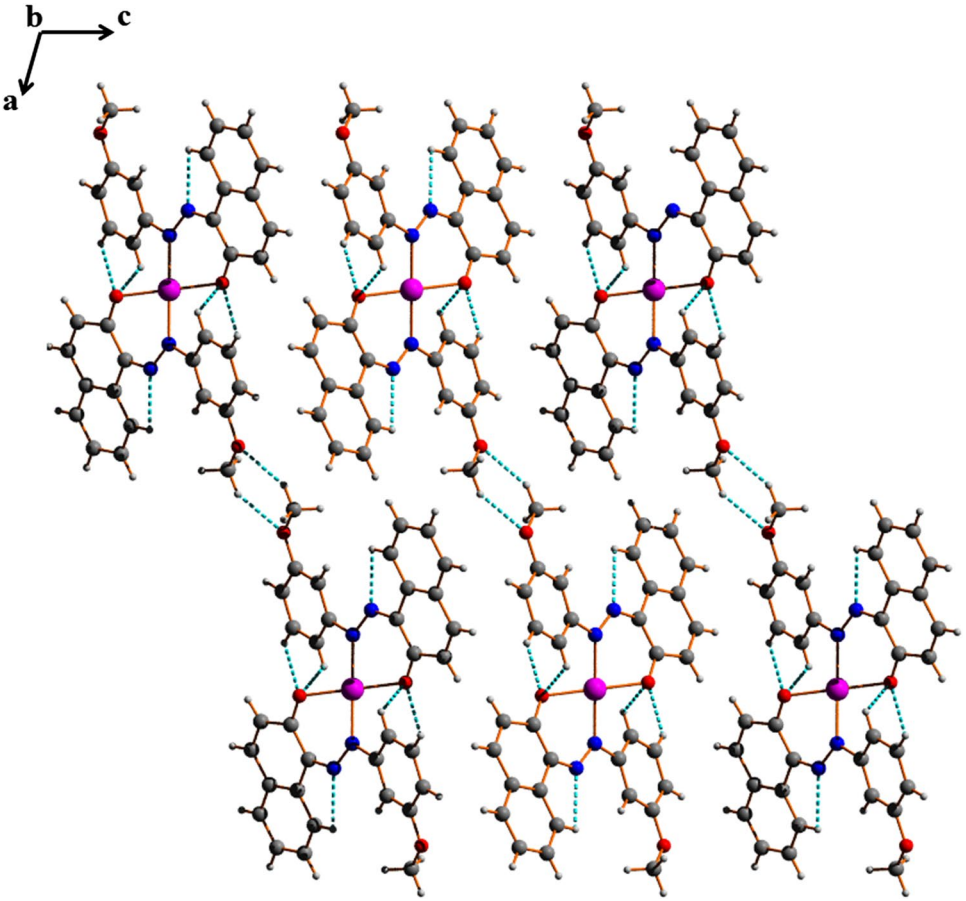

Fig. 4 A partial view along the b axis of the crystal packing of the title complex (II), showing the C–H···N and C–H···O interactions which are displayed as dashed lines (see Table 3)

is related to that of the free ligand and also to O···O repulsions that occur between the oxygen atom of each methoxy group (NAO charge = −0.50) and the oxygen atom directly bound to the Pd center (NAO charge = −0.65) [47, 48]. In (I), the oxygen atoms displaying negative charges are face-to-face, hence, leading to electrostatic repulsions. Due to the described repulsions, (I) is destabilized by 12.0 and 11.5 kcal/mol with respect to (II) and (III), respectively. Indeed in these two isomers, the methoxy and the azo groups are in remote positions to each other decreasing the repulsion interactions. Nevertheless, in the three complexes the metal adopts a nearly square-planar conformation (Fig. 8 and Table 4), with ONON dihedral angles of 0°, 0°and 2° for (I), (II) and (III), respectively. The square-planar environment

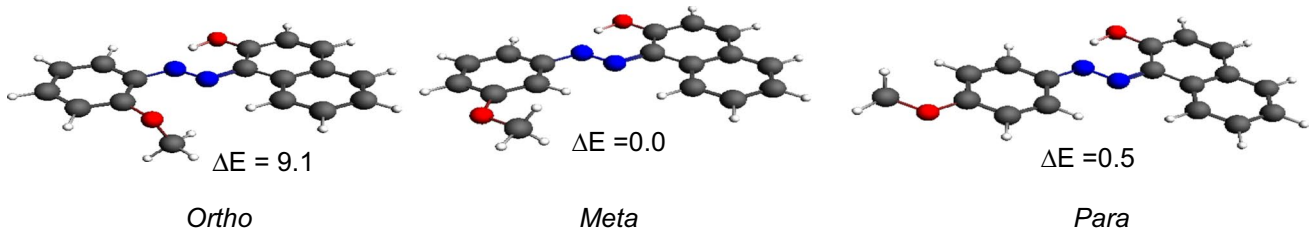

Fig. 5 Optimized structures obtained for the free ligand precursor isomers. Relative energies ΔE are given in kcal/mol

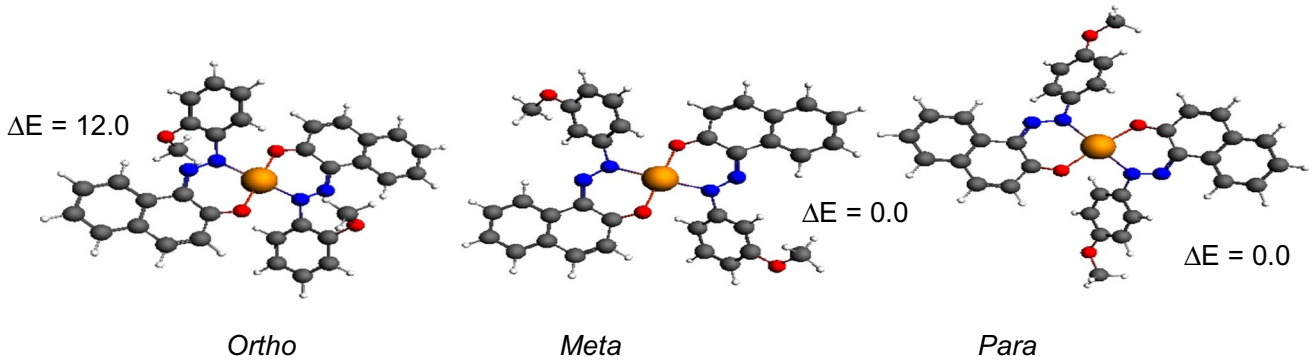

Fig. 6 Optimized structures obtained for complexes (I), (II) and (III) in their singlet ground state. Relative energies between isomers ΔE are given in kcal/mol

Table 4 Selected geometrical and energetic parameters obtained for (I), (II) and (III). Experimental values are given in parentheses. Bond distances are given in Å

	Free ligand			Complex		
Isomer	*Ortho*	*Meta*	*Para*	(I)	(II)	(III)
ΔE (kcal/mol)	9.1	0.0	0.5	12.0	0.0	0.0
HOMO–LUMO gap (eV)	1.89	1.85	1.86	1.72	1.57	1.51
N1-N2	1.292	1.292	1.291	1.277 (1.282)	1.270 (1.274)	1.278
Average C–C (phenyl)				1.391 (1.389)	139.0 (1.387)	1.391 (1.385)
Average C–C (naphthyl)				1.400 (1.396)	141.2 (1.403)	140.3 (1.400)
C–O (methoxy)				1.367 (1.367)	1.374 (1.372)	1.373
Pd–N(Å)	–	–	–	2.082 (1.976)	2.106 (2.031)	2.114
Pd–O (Å)	–	–	–	2.071 (2.004)	2.069 (2.000)	2.069
N2-Pd-N2^{i} (°)	–	–	–	180.0 (180.0)	180.0 (180.0)	178.0
O1-Pd-O1^{i} (°)	–	–	–	180.0 (180.0)	180.0 (180.0)	179.0
O1-Pd-N2				(89.69)	87.3 (86.41)	
O1-Pd-N2^{i}				(91.31)	92.7 (93.56)	
N2-O1-N2^{i}-O1^{i} (°)				0 (0)	0 (0)	2
Natural Pd population (NBO)	–	–	–	+0.80	+0.79	+0.76

of the d^8 Pd(II) center in the three complexes (Fig. 8) was expected, owing to its 16-MVE (metal valence electrons) configuration.

Steric effects can be evidenced by the orientation between the phenyl and naphthyl rings around the azo group. The largest distortion is observed for (I), due to repulsions between the azo groups of both ligands. This distortion decreases for (II) and (III), whose relative stability is depending on the position of the methoxy group. The optimized Pd–N and Pd–O bond distances for (I) and (II) are comparable to those observed experimentally, where the differences do not exceed 0.07 Å (Table 4). They are also comparable to those reported in the literature of related complexes [49, 50]. The C–C bond distances ranging from 1.38 to 1.42 Å suggest delocalization within the phenyl and naphthyl. They are comparable to those found in previous works [51–57].

The large HOMO–LUMO gaps of 1.72, 1.57 and 1.51 eV of (I), (II) and (III), respectively, are consistent with a good kinetic stability. Kohn–Sham MO plots of the three complexes are displayed in Fig. 7. They show substantial resemblance. Their HOMOs are localized on the Pd center, with antibonding ligand admixture. Their LUMOs are ligand based, with antibonding N–N and O–O characters.

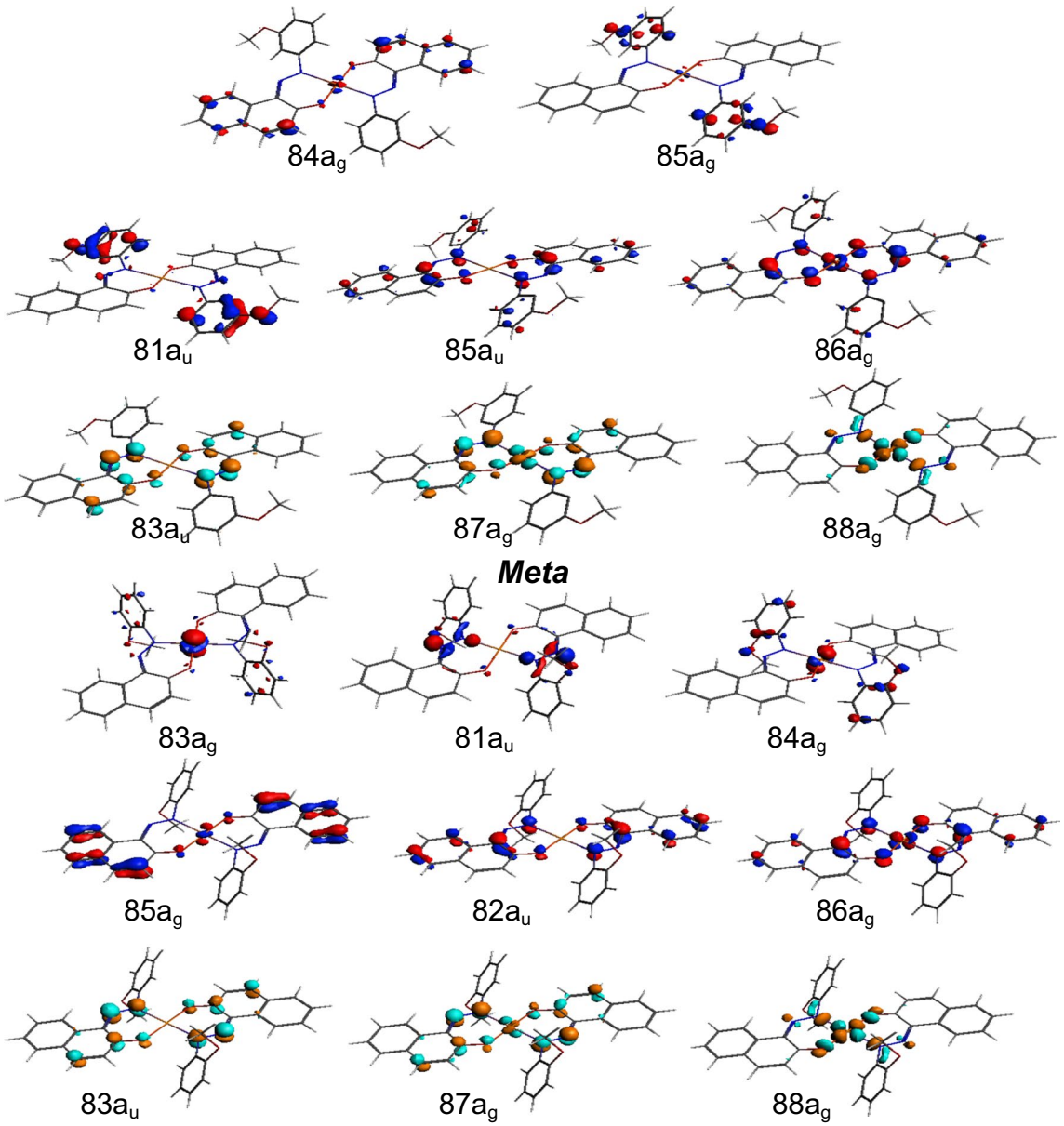

Fig. 7 MO plots of the crucial orbitals for (I) (top) and (II) (bottom) isomers. For both complexes (I) and (II), the HOMO and LUMO correspond to $86a_g$ and $83a_u$ MOs, respectively

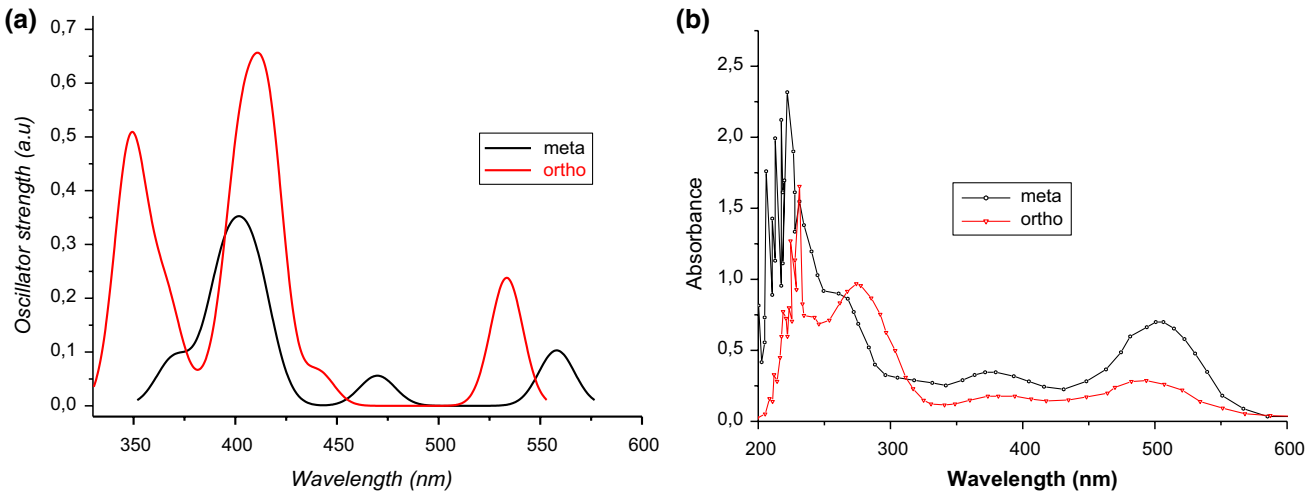

Fig. 8 TD-DFT simulated (**a**) and experimental (**b**) UV–Vis spectra for complexes (I) and (II) in CH_2Cl_2

UV–Vis electronic spectra

TD-DFT calculations [45] were carried out on (I) and (II), taking into account solvent (CH_2Cl_2) effects (see computational details). Their simulated electronic spectra (Fig. 8a) show some differences which are somewhat influenced by the methoxy position. They also were found to be extremely sensitive to their environment, such as the solvent polarity, as known for many dye molecules [57–59]. The simulated spectra are in good agreement with their experimental counterparts (Fig. 8b). Because of the different conjugative effects in their respective ligands, different electronic transitions are expected to occur in I and II. They were assigned from our TD-DFT results and the orbitals shown in Fig. 7.

The main calculated absorption bands of 0.52 a.u is centered at 348 nm, corresponding to the experimental one at 381 nm. It is an intense HOMO-3($84a_g$) → LUMO + 2($84a_g$) transition of (d(M) + π (L)) → π *(L) nature. Thus, The main band is the result of a strong intra-ligand charge transfer (ILCT) associated with ligand-to-metal charge transfer (LMCT). The second main band of 0.65 a.u can be identified as a HOMO($86a_g$) → LUMO($83a_u$) transition of MLCT character. The band found at relatively low energy and centered at 534 nm (experimental at 515 nm) is mainly a HOMO($86a_g$) → LUMO ($83a_u$) transition corresponding to a metal-to-ligand charge transfer (MLCT).

The simulated electronic spectrum of (II) shows only one major broad peak centered at 400 nm, which is less intense than those obtained for (I). This peak is composed of two transitions: one appears at 394 nm and the other one at 408 nm, comparable to the experimental one which is found at 382 nm. The first peak corresponds to a mixture of HOMO-4($84a_g$) → LUMO($83a_u$) (65%) and HOMO-5($83a_g$) → LUMO($83a_u$) (36%) transitions. They are of intra-ligand (ILCT) and ligand-to-metal (LMCT) charge transfer character. The second peak corresponds to HOMO-1($82a_u$) → LUMO + 2($88a_g$) (40%), HOMO-3($81a_u$) → LUMO + 1($87a_g$) (30%) and HOMO-4($85a_g$) → LUMO($83a_u$) (20%) transitions giving rise to ligand-to-metal charge transfer (LMCT). Finally, both bands appearing at 558 nm (experimentally centered at 510 nm) are of weak intensities and are of LMCT character.

Conclusion

This paper reports the preparation, the spectroscopic analyses, X-ray characterization and theoretical calculations of two palladium complexes (I) and (II) containing azo dye ligands. Both complexes (I) and (II) exhibit a square planar geometry around the metal, and the solid-state supramolecular structures are maintained by π-stacking interactions. The weak intermolecular interactions observed in the solid state do not distort the molecular structures significantly. The DFT-optimized structures of (I) and (II) reproduce well the structural properties of their experimentally determined X-ray counterparts. Complexes (I), (II) and (III) display large HOMO–LUMO gaps, in line with the strong metal–ligand interactions. Complex (I) is computed to be less stable by 12.0 and 11.5 kcal/mol than (II) and (III), respectively, showing the impact of the methoxy position on the molecular structures, which are planar in (II) and (III), but distorted in (I). The simulated UV–Vis spectra obtained by TD-DFT calculations are comparable to the experimental spectra, putting emphasis on the ILCT and MLCT electronic transitions involving several of the frontier molecular orbitals in the complexes.

Author contributions The manuscript was written through contribution of all authors. All authors have given approval to the final version of the manuscript.

Funding The authors received financial support from the Algerian MESRS (Ministère de l'Enseignement Supérieur et de la RechercheScientifique) and DGRSDT (Direction Générale de la Recherche Scientifique et du Développement Technologique).

Compliance with ethical standards

Conflict of interest The authors declare that they have no competing interest.

References

1. Dharmalingam V, Ramasamy AK, Balasuramanian V (2011) Synthesis and EPR studies of copper metal complexes of dyes derived from remazol red B, procino yellow, fast green FCF, brilliant cresyl blue with copper acetate monohydrate. E-J Chem 8:S211–S224
2. Khedr AM, Gaber M, Abd El-Zaher EH (2011) Synthesis, structural characterization, and antimicrobial activities of Mn(II), Co(II), Ni(II), Cu(II) and Zn(II) complexes of triazole-based azodyes. Chin J Chem 29:1124
3. Kirkan B, Gup R (2008) Synthesis of new Azo dyes and copper(II) complexes derived from Barbituric acid and 4-Aminobenzoyl hydrazone. Turk J Chem 32:9–17
4. Sekar N (1999) Ecofriendly metal complex dyes an update. Colourage 46:63–65
5. Thomas AM, Nethaji M, Chakravarty ARJ (2004) Different modes of DNA cleavage activity of dihydroxo-bridged dicopper (II) complexes having phenanthroline bases. Inorg Biochem 98:1087–1097
6. Reed JE, Arnal AA, Neidle S, Vilar R (2006) Stabilization of G-quadruplex DNA and inhibition of telomerase activity by square-planar nickel (II) complexes. J Am ChemSoc 128:5992–5993
7. Selvakumar B, Rajendiran V, Uma Maheswari P, Stoeckli-Evans H, Palaniandavar M (2006) Structures, spectra, and DNA-binding properties of mixed ligand copper(II) complexes of iminodiacetic acid: the novel role of diimine co-ligands on DNA conformation and hydrolytic and oxidative double strand DNA cleavage. J Inorg Biochem 100:316–330
8. Patra AK, Nethaji M, Chakravarty AR (2007) J Synthesis, crystal structure, DNA binding and photo-induced DNA cleavage activity of (S-methyl-L-cysteine)copper(II) complexes of heterocyclic bases. Inorg Biochem 101:233–244
9. Chen GJ, Qiao X, Qiao PQ, Xu GJ, Xu JY, Tian JL, Gu W, Liu X, Yan SP (2010) Synthesis, DNA binding, photo-induced DNA cleavage, cytotoxicity and apoptosis studies of copper(II) complexes. J Inorg Biochem 105:119–126
10. Cvek B, Milacic V, Taraba J, Dou QP (2008) Ni (II), Cu (II), and Zn (II) diethyldithiocarbamate complexes show various activities against the proteasome in breast cancer cells. J Med Chem 51:6256–6258
11. Abe T, Mano S, Yamaya Y, Tomotake A (1999) Thermal dye transfer printing with chelate compounds. J Imag Sci Tech 43:339–344
12. Meyers GA, Michaels FM, Reeves RL, Trotter P (1985) Kinetics and mechanism of chelation of nickel(II) by a tridentate alpha.-[(2-hydroxyphenyl)azo]-alpha.-acetoacetonitrile and an alpha.-(8-quinolylazo)-.alpha.-acetoacetonitrile dye. J InorgChem 24:731–738
13. Graves HM, Johnston LG, Reiser A (1988) The effect of metallization on singlet oxygen formation by azo dyes. J PhotochemPhotobiolA 43:183–192
14. Liu JC-I, Bailar JC Jr (1998) The structures and properties of lakes of some azo dyes. InorgChimActa 145:181–184
15. Woodward C, Freiser H (1973) Sulphonated azo-dyes as extractive metallochromic reagents. Talanta 20:417–420
16. Shibata S, Furukawa M, Toei K (1973) Syntheses and spectrophotometric studies of azo dyes containing m-dimethylaminophenol as analytical reagents. Anal ChimActa 66:397–409
17. Pilipenko AT, Savransky LI (1987) Selectivity and sensitivity of metal determination by co-ordination compounds. Talanta 34:77–86
18. Szurdoki F, Ren D, Walt DR (2000) A combinatorial approach to discover new chelators for optical metal ion sensing. Anal Chem 72:5250–5257
19. Wang S, Shen S, Xu H (2000) Synthesis, spectroscopic and thermal properties of a series of azo metal chelate dyes. Dyes Pigments 44:195–198
20. Park HY, Lee NH, Je JT, Min KS, Huh YJ, Kim E-R (2001) Synthesis and Characterization of X-azo Dyes (X=Ni, Cu, Zn) for Digital Versatile Disc-Recordable (DVD-R). MolCrystLiqCryst 371:305–308
21. Park H, Kim E-R, Kim DJ, Lee H (2002) Synthesis of metal-azo dyes and their optical and thermal properties as recording materials for DVD-R. Bull ChemSocJpn 75:2067–2070
22. Pratihar JL, Mandal P, Lin CH, Lai CK, Mal D (2017) Azoamide palladium(II) complexes: synthesis, characterization and application in C-C cross-coupling reactions. Polyhedron. https://doi.org/10.1016/j.poly.2017.06.055
23. Munusamy S, Muniyappan P, Galmari V (2019) Synthesis and structural characterization of palladium(II) 2-(arylazo)naphtholate complexes and their catalytic activity in Suzuki and Sonogashira coupling reactions. J CoordChem 72:1910–1921
24. Jana S, Chandan RN, Manna K, Mondal TK (2020) Synthesis, characterization, X-ray structure and DNA binding study of palladium(II) complex with new thioether containing ONS donor ligand. J ChemSci 132:64–72
25. Pratihar P, Mondal TK, Patra AK, Sinha C (2009) trans-Dichloro-bis-(arylazoimidazole)palladium(II) azo-N to make free azo (-NdN-) function is important to reveal photochromic activity. Inorg Chem 48:2760–2769
26. Sen C, Roy S, Mondal TK, Ghosh R, Mondal JA, Palit DK, Sinha C (2015) Palladium(II)-iodo-{1-alkyl-2-(arylazo)imidazole} complexes: Synthesis, structure, dynamics of photochromism and DFT computation. Polyhedron 85:900–911
27. Salmen R, Malterud KE, Pedersen BF (1988) Acta Chem. Scand A 42:493
28. Gilli P, Bertolasi V, Pretto L, Antonov L, Gilli G (2005) J Am Chem Soc 127:4943
29. Sheldrick GM (2008) A shrt history of SHELX. Acta Cryst A64:112–122
30. Sheldrick GM (2015) Crystal structure refinement with SHELXL. Acta Cryst C71:3–8
31. Farrugia LJ (2012) WinGX and ORTEP for Windows: an update. J Appl Cryst 45:849–854
32. ADF2016.01 (2016) Version Theoretical Chemistry Vrije Universiteit Amsterdam, The Netherlands, SCM
33. Baerends EJ, Ellis DE, Ros P (1973) Self-consistent molecular Hartree-Fock-Slater calculations I. Comput Proc Chem Phys 2:41
34. teVelde G, Baerends EJ (1992) Numerical integration for polyatomic systems. J Comput Phys 99:84
35. Fonseca Guerra C, Snijders JG, teVelde G, Baerends EJ (1998) Towards an order-N DFT method. The ChimAcc 99:391

36. Bickelhaupt FM, Baerends EJ (2000) Kohn-Sham density functional theory: predicting and understanding chemistry. Rev ComputChem 15:1
37. teVelde G, Bickelhaupt FM, Fonseca Guerra C, van Gisbergen SJA, Baerends EJ, Snijders JG, Ziegler T (2001) Chemistry with ADF. J ComputChem 22:931
38. Becke AD (1993) Density functional thermochemistry.III. The role of exact exchange. J Chem Phys 98:5648
39. Lee C, Yang W, Parr RG (1998) Development of the Colle-Salvetti correlation-energy formula into a functional of the electron density. Phys Rev B 37:785
40. vanLenthe E, Baerends EJ, Snijders JG (1993) Relativistic regular two-component Hamiltonians. J Chem Phys 99:4597–4610
41. vanLenthe E, Baerends EJ, Snijders JG (1994) Relativistic total energy using regular approximations. J Chem Phys 101:9783–9792
42. vanLenthe E, Baerends EJ, Snijders JG (1999) Geometry optimizations in the zero order regular approximation for relativistic effects. J Chem Phys 110:8943–8953
43. Fan L, Ziegler T (1992) Application of density functional theory to infrared absorption intensity calculations on main group molecules. J Chem Phys 96:9005
44. Fan L, Ziegler T (1992) Application of density functional theory to infrared absorption intensity calculations on transition-metal carbonyls. J Chem Phys 96:6937
45. Runge E, Gross EKU (1984) Density-functional theory for time-dependent systems. Phys Rev Lett 52:997–1000
46. Klamt A, Schüümann G (1993) COSMO: a new approach to dielectric screening in solvents with explicit expressions for the screening energy and its gradient. J ChemSoc Perkin Trans 2:799–805
47. Weinhold F, Landis CR (2005) Valency and bonding: a natural bond orbital donor–acceptor perspective. Cambridge University Press, Cambridge
48. Weinhold F, Glendening ED (2001) NBO 5.0 program manual: natural bond orbital analysis programs. University of Wisconsin, Madison, Theoretical Chemistry Institute and Department of Chemistry
49. Chetioui S, Rouag DA, Djukic JP, Bochet CG, Touzani R, Bailly C, Crochet A, Fromm KM (2016) Crystal structures of a copper(II) and the isotypic nickel(II) and palladium(II) complexes of the ligand (E)-1-[(2,4,6-tribromophenyl)diazenyl]naphthalen-2-ol. Acta Cryst E 72:1093
50. Lin ML, Tsai CY, Li CY, Huang BH, Ko BT (2010) Bis{1-[(E)-(2-methyl-phen-yl)diazen-yl]-2-naphtho-lato}palladium(II). Acta Cryst E 66:m1022
51. MerzougM ZB (2014) Coordination diversity of the phenazine ligand in binuclear transition metal sandwich complexes: theoretical investigation. J Organomet Chem 770:69–78
52. KorichiH ZouchouneF, ZendaouiSM ZouchouneB, Saillard JY (2010) The coordination chemistry of azulene: a comprehensive DFT investigation. Organometallics 29:1693–1706
53. ZendaouiSM ZouchouneB (2013) Molecular properties and electronic structure of phenazine ligand in binuclear molybdenum and manganese metal complexes: a density functional theory study. Polyhedron 51:123–131
54. Bouchakri N, Benmachiche A, Zouchoune B (2011) Bonding analysis and electronic structure of transition metalbenzoquinoline complexes: a theoretical study. Polyhedron 30:2644–2653
55. ZouchouneB MerzougM (2019) BensalemN. Struct Chem. https://doi.org/10.1007/s11224-019-01322-z
56. Ababsa S, Farah S, Zouchoune B, Benhamada N (2010) Theoretical investigation of the coordination of dibenzazepine to transition-metal complexes. Polyhedron 29:2722–2730
57. Mkpenie VN, Essien EE (2015) Solvent and methyl group effects on the electronic spectral properties of azo-2-naphtol dye. Am ChemSci J 8:1–8
58. Zouchoune B, Mansouri L (2019) Electronic structure and UV–Vis spectra simulation of square planar Bis (1-(4-methylphenylazo)-2-naphtol)-Transition metal complexes [M(L)2]x (M= Ni, Pd, Pt, Cu, Ag, and x = − 1, 0, + 1): DFT and TD-DFT study. StructChem 30:691–701
59. Mansouri L, Zouchoune B (2015) Substitution effects and electronic properties of the azo dye (1-phenylazo-2-naphthol) species: a TD-DFT electronic spectra investigation. Can J Chem 93:509–517